Proc. AFI/TFI-2004, November 11-12, 2004, Sendai, Japan, pp. 346-351

Feedback Control of Near-Wall Reynolds Shear Stress in Wall-Turbulence

Koji FUKAGATA* and Nobuhide KASAGI*

A new idealized control scheme is proposed for drag reduction in wall-turbulence and its effects are studied by means of DNS of turbulent pipe flow. The control input is given as a function of sensed streamwise velocity fluctuation above the wall in order to suppress the near-wall Reynolds shear stress, which is directly related to the turbulent skin friction drag [Fukagata et al., Phys. Fluids, Vol. 14 (2002), p. L73-L76]. A significant amount of drag reduction, which compares well with the opposition control [Choi et al., J. Fluid Mech., Vol. 262 (1994), p. 75-110], is obtained. Effects of deteriorated sensor signals are also investigated. With the present control scheme, the drag reduction rate is kept at the same level as long as the correlation coefficient between the original and deteriorated signals is higher than 0.5.

Key Words : Turbulence, Control, Skin Friction Drag, Direct Numerical Simulation, Reynolds Shear Stress

1. Introduction

Active feedback control is expected as a technique to flexibly manipulate wall-bounded turbulent flows appearing in industrial applications. Owing to the maturity of numerical simulation techniques and increased understanding of wall-turbulence, a variety of studies have been made on the active feedback control in the last decade, especially on the control schemes for skin friction drag reduction[(1) (2)].

Control schemes rigorously based on the modern control theory, such as the optimal control theory, are suitable for studying the potential of turbulence control. Recently, Bewley et al. [(3)] demonstrated in their direct numerical simulation (DNS) that a channel flow at $Re_\tau = 100$ can be relaminarized by the optimal control. Implementation of the optimal control scheme in real applications, however, is probably impossible because the state information should be known in the entire flow domain and extremely large computational resource is required to determine the control input.

Several attempts have been made to develop practical control schemes based on physical arguments. As is well-known, the increase of skin-friction drag in turbulent wall-bounded flow is closely associated with so-called quasi-streamwise vortices (QSVs). Therefore, the most common strategy for the physical argument-based drag reduction control schemes is attenuation of these QSVs. Choi et al. [(4)] proposed a very simple QSV-based control scheme, i.e., the opposition control, in which the blowing/suction velocity at the wall is set opposite to the wall-normal velocity in a plane y_d above the wall (sensed by virtual sensors), i.e.,

$$v(x,0,z,t) = -v(x,y_d,z,t)\,. \tag{1}$$

Despite its simplicity, more than 20 % of skin friction drag was reduced in DNSs of channel flow at the friction Reynolds number of $Re_\tau = 100 - 650$ [(4)~(6)], and pipe flow at $Re_\tau = 180$ [(7)]. In order to meet the requirements in real applications, Lee et al. [(8)] and Lee et al. [(9)] developed control schemes requiring the information at walls only in the framework of QSV-based approach. About 22 % drag reduction was achieved in their DNS of channel flow at $Re_\tau = 100$ by applying the derived control law that uses spanwise wall shear information.

Recently, Fukagata et al. [(10)] analytically derived a direct relationship between the Reynolds shear stress (RSS) and the skin friction coefficient ($C_f = \overline{\tau_w^*}/[(1/2)\rho^* U_b^{*2}]$) under the condition of constant flow rate. For instance, the relationship for the fully developed channel flow reads

$$C_f = \frac{12}{Re_b} + 12\int_0^1 2(1-y)(-\overline{u'v'})\,dy\,. \tag{2}$$

Here, all variables without superscript are those non-dimensionalized by the channel half width, δ^* and twice the bulk mean velocity, $2U_b^*$, while the dimensional variables are denoted by the superscript of $*$. The bulk Reynolds number is defined as $Re_b = 2U_b^*\delta^*/\nu^*$. The overbar ($\bar{\cdot}$) and prime ($\cdot'$) denote the mean and fluctuation components of the Reynolds decomposition. This relationship is also valid under the control by local blowing/suction from walls and it suggests that the RSS should be suppressed near the wall in order to reduce the

*Department of Mechanical Engineering, The University of Tokyo, Hongo 7-3-1, Bunkyo-ku, Tokyo 113-8656, Japan. E-mail: fukagata@thtlab.t.u-tokyo.ac.jp (K. Fukagata)

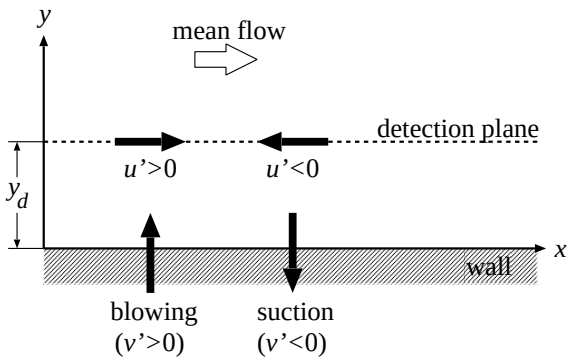

Fig. 1 Schematic of the present control scheme.

skin friction drag.

Following this finding, we proposed a cost function based on the suppression of RSS near the wall[11], and derived an analytical suboptimal solution for that cost function by applying the derivation procedure proposed by Lee et al.[9]. The derived control law requires only the streamwise wall shear signal, which can be measured with a sufficient accuracy by using an advanced wall shear stress sensor [12]. However, the drag reduction rate achieved in the DNS of turbulent pipe flow at $Re_b = 5300$ (i.e., $Re_\tau = 180$ for uncontrolled flow) was 11 % [11]. The reason for this small amount of drag reduction is likely that they estimated the Reynolds shear stress above the wall from the wall shear stress by using a low-order Taylor series expansion.

We believe that higher drag reduction rate is attainable with the RSS-based approach if the velocity above the wall is more accurately estimated from the information available at the wall. Recently, such attempts to accurately estimate the flow variables from the wall information have been reported by several researchers [13]~[15], although the estimation has been made so far only for uncontrolled flows. Especially, Milano and Koumoutsakos[13] demonstrated that, by using a nonlinear neural network in an ordinary (i.e, uncontrolled) channel flow, the streamwise (u) and wall-normal (v) velocities near the wall can be accurately estimated from the wall information. The correlation coefficient C between the estimated and true values at the height of $y^+ = 15$ is very high for u ($C = 0.9$), and fairy high for v ($C = 0.6$). Therefore, if there is an efficient control scheme which uses the information of streamwise velocity fluctuation above the wall, it can be implemented in the practical system in combination with advanced state estimation techniques.

In the present study, we propose such an idealized control scheme, which uses the streamwise velocity above the wall as a sensor information. The control input is determined so as to suppress the RSS. In addition to cases where the streamwise velocity above the wall is perfectly known, cases with artificially deteriorated sensor signals are also studied. The latter mimics the practical situation where the streamwise velocity above the wall is estimated by using the information available on the wall.

Table 1 Number of grids (N_r, N_θ, N_z) and grid spacing (Δr, $R\Delta\theta$, Δz) used in DNS of pipe flow.

N_r	N_θ	N_z	Δr^{+u}	$(R\Delta\theta)^{+u}$	Δz^{+u}
48	128	256	0.95 - 6.11	9.03	14.4

2. Control Scheme

The control input is introduced as blowing/suction from the wall. In order to suppress the RSS above the wall, we propose the following intuitive control scheme:

$$v(x,0,z,t) = \alpha\, u'(x,y_d,z,t) \tag{3}$$

in the Cartesian coordinates (x,y,z) and

$$u_r(0,\theta,z,t) = -\alpha\, u'_z(R-y_d,\theta,z,t) \tag{4}$$

in the cylindrical coordinates (r,θ,z). The sensed signal is the streamwise velocity fluctuations, u', in a plane y_d away from the wall. The blowing/suction velocity is proportional to u' with an amplitude factor, α. The schematic of the present control scheme is shown in Fig. 1.

As mentioned in Introduction, the velocity above the wall in real applications should be estimated from the information available at the wall. In this case, the virtual sensor signal ($u'(x,y_d,z,t)$ or $u'_z(R-y_d,\theta,z,t)$) is simply replaced by the estimated velocity, denoted as $\tilde{u}'$. The relation between true and estimated velocities may depend on the method of state estimation. In the present study, we assume an ideal case where the intensity of spatial spectra is correctly estimated, but the phase of them contain errors. Namely, we model the estimated velocity $\tilde{u}'$ as an original velocity with a random phase shift, i.e.,

$$\widehat{\tilde{u}} = \widehat{u}\, e^{i\sigma n}, \tag{5}$$

where $\widehat{\cdot}$ denotes the two-dimensional (i.e., streamwise and spanwise) Fourier transform, σ is the standard deviation of the phase shift, and n is the zero-mean Gaussian random number with unit variance.

3. Numerical Procedure

Effectiveness of the above-mentioned control scheme is investigated by means of direct numerical simulation (DNS) of turbulent pipe flows. The DNS code is based on the energy conservative finite difference method for the cylindrical coordinate system [16]. The time

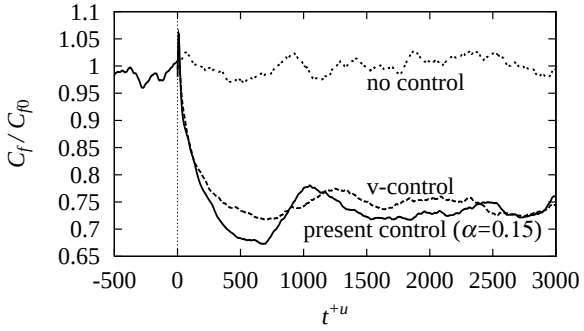

Fig. 2 Time trace of normalized skin friction coefficient. Detection plane is $y_d^{+u} \simeq 15$.

integration is done by using the low storage third-order Runge-Kutta/Crank-Nicolson scheme[17] coupled with the higher-order fractional step method[18]. The bulk mean velocity is kept constant and the Reynolds number is $Re_b = 5300$ (i.e., $Re_\tau \simeq 180$ for uncontrolled flow).

The computational domain has a longitudinal length of $L = 20R$ and the periodic boundary conditions are applied at both ends. The specification of the computational grid is summarized in Table 1. Here, the superscript of $+u$ denotes the wall unit of the uncontrolled flow. Although the grid system used is not very fine, it has been verified in the previous DNS of opposition controlled flows[7] that this grid resolution is sufficient to evaluate the drag reduction rate.

4. Results and Discussions

First, analysis is made on the cases of the accurate sensor signal, i,e., Eq. (4). Figure 2 shows the time trace of the skin friction coefficient, C_f, normalized by that in the uncontrolled flow, C_{f0}. The present control is compared with the opposition control[4] (hereafter referred to as *v*-control) of the pipe flow under the same conditions[7]. Here, the detection plane is $y_d^{+u} \simeq 15$ for both control schemes. The amplitude factor for the present control scheme is $\alpha = 0.15$. The transient behavior of C_f with the present control is essentially similar to that with *v*-control; C_f slightly increases in the initial stage, then significantly drops, and finally reaches a quasi-steady state after $t^{+u} = 1000$. With the present control, the maximum drag reduction rate during this initial stage is slightly larger ($R_{D,max} = 33$ %) than the case with *v*-control ($R_{D,max} = 27$ %).

Dependency of the average drag reduction rate in the quasi-steady state (R_D) on the detection plane height (y_d^{+u}) is shown in Fig. 3. The maximum average drag reduction is $R_D = 27$ %, which is comparable to that in *v*-control, and it is attained with $y_d^{+u} \simeq 15$ and $\alpha = 0.15$. The dependency of R_D on y_d^{+u} is also similar to *v*-control. The drag reduction effect is weakened for the detection

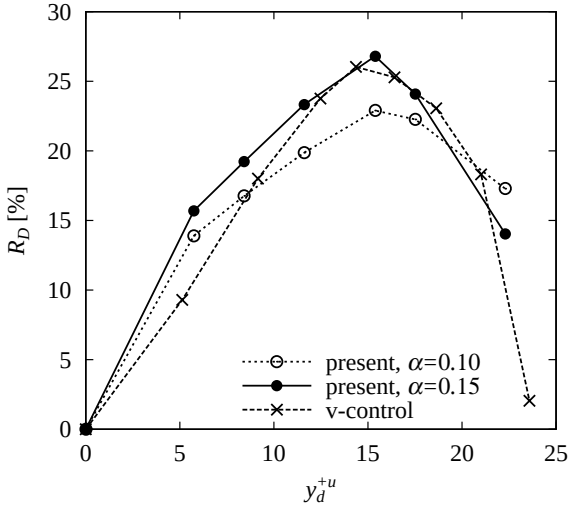

Fig. 3 Drag reduction rate, R_D, versus detection plane height, y_d^{+u}.

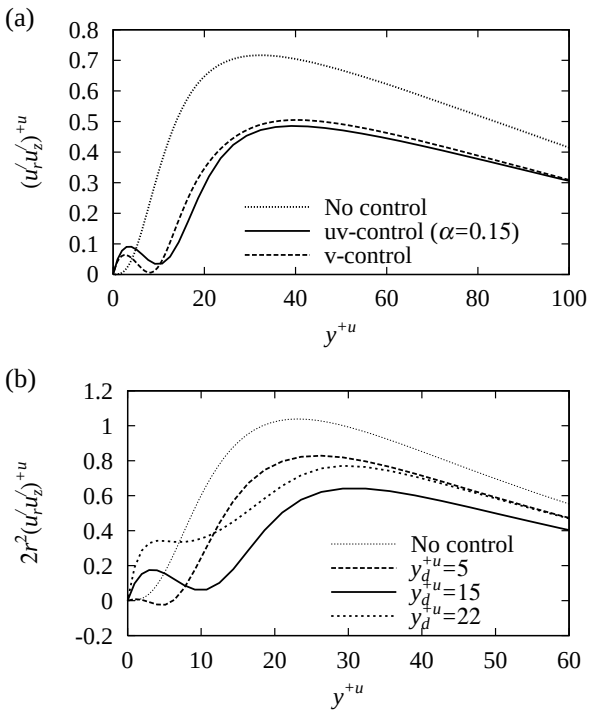

Fig. 4 Weighted Reynolds shear stress. (a) Comparison between present control (uv-control) and opposition control (v-control) with detection plane at $y_d^{+u} \simeq 15$; (b) Present control ($\alpha = 0.15$) at different detection plane heights.

plane higher than $y_d^{+u} \simeq 15$. Note that no drag reduction effect was obtained in the cases of $\alpha > 0.15$. In those cases, C_f increased in the initial stage, similarly to Fig. 2, but C_f did not entered into the subsequent decreasing phase.

Figure 4 shows the profiles of weighted Reynolds shear stress (RSS) appearing in the turbulent contribution term

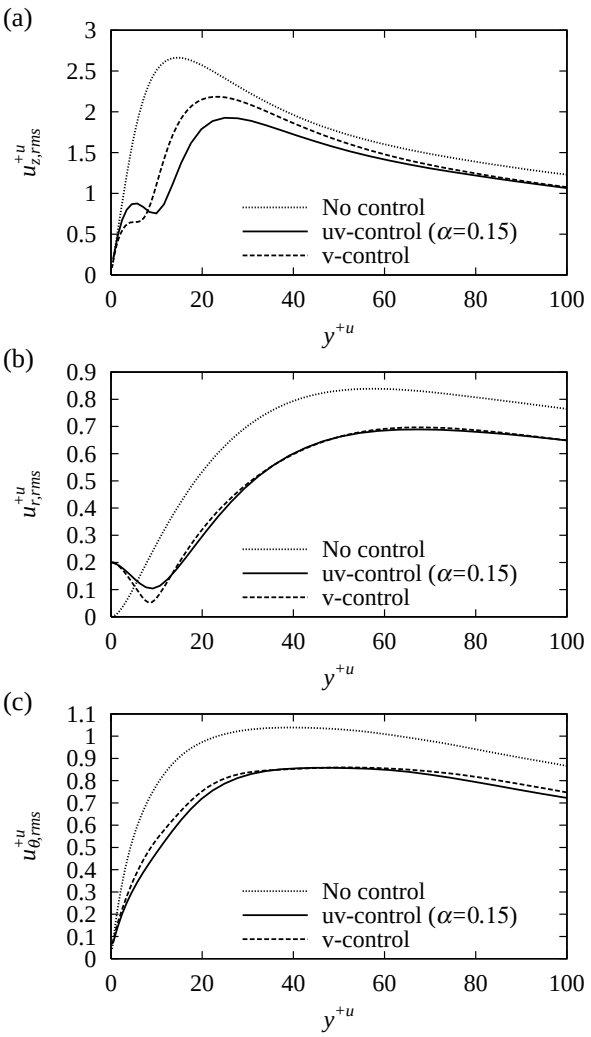

Fig. 5 Rms velocities with present control (uv-control) and opposition control (v-control). Detection plane is $y_d^{+u} \simeq 15$. (a) longitudinal; (b) radial; (c) azimuthal.

in the integral relation, Eq. (2), which reads

$$C_f = \frac{16}{Re_b} + 16 \int_0^1 2r\, \overline{u_r' u_z'}\, r dr \,, \qquad (6)$$

for pipe flows. Similarly to the case of *v*-control (see, Fig. 4(a)), RSS is directly suppressed near the wall ($y^{+u} \simeq 10$), and it leads to significant reduction of turbulent contribution to C_f together with the indirect suppression[7] of RSS far from the wall. In the case of $y_d^{+u} \simeq 5$ (Fig. 4(b)), the weighted RSS takes a slightly negative value near the wall ($y^{+u} \simeq 5$), which is similar to the case of RSS-based suboptimal control[11]. The location that gives the minimum value of weighted RSS, however, is too close to the wall to result in smaller indirect suppression[7] of RSS far from the wall, and hence the smaller drag reduction effect. For $y_d^{+u} \simeq 22$, there is no local minimum in the profile of weighted RSS. The direct effect of control seems to extend up to

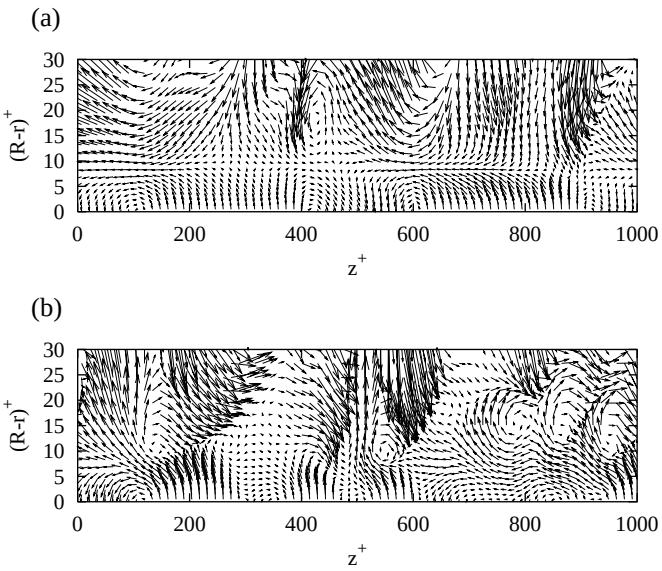

Fig. 6 Typical instantaneous velocity fluctuation vectors in $r-z$ plane. (a) opposition control ($y_d^{+u} \simeq 15$); (b) present control ($y_d \simeq 15$, $\alpha = 0.15$).

$y^{+u} \simeq 20$. The amount of suppression in the weighted RSS, however, is smaller and thus the drag reduction rate is smaller.

Figure 5 show the root-mean-square (rms) velocity fluctuations. The profiles in the case of present control are essentially similar to those in *v*-control. Slight differences can be noticed in the streamwise ($u_{z,rms}$) and wall-normal ($u_{r,rms}$) components. As compared to *v*-control, the direct effect of control on $u_{z,rms}$ is found farther from the wall, whereas the suppression of $u_{r,rms}$ around $y^{+u} = y_d^{+u}/2$, which causes the formation of a virtual wall[5], is milder.

Although the effects of present control are statistically similar to those of *v*-control, a clear difference is observed in the velocity field. Figure 6 shows typical instantaneous velocity vectors, $(u_z', -u_r')$, in a longitudinal (streamwise)-radial (wall-normal) plane. With *v*-control, a distinct virtual wall[5] is formed around $y^{+u} \simeq y_d^{+u}/2 \simeq 8$. The fluctuating velocity vectors are nearly symmetric around the virtual plane. The situation is essentially the same in other realizations. With the present control, in contrast, there are substantially many regions where the virtual wall is not formed. Because the control scheme is designed so that blowing is applied for positive u_z' above the wall, the velocity fluctuation vectors below and above $y^{+u} \simeq 10$ are nearly perpendicular to each other in some regions (e.g., around $z^{+u} = 200$ and $z^{+u} = 400$ in Fig 6(b)), or strong spanwise vortices are created in some other regions (e.g., around $z^{+u} = 550$ and $z^{+u} = 800 - 1000$ in Fig 6(b)).

Up to now, we have investigated the effects of present idealized RSS-based control by assuming that

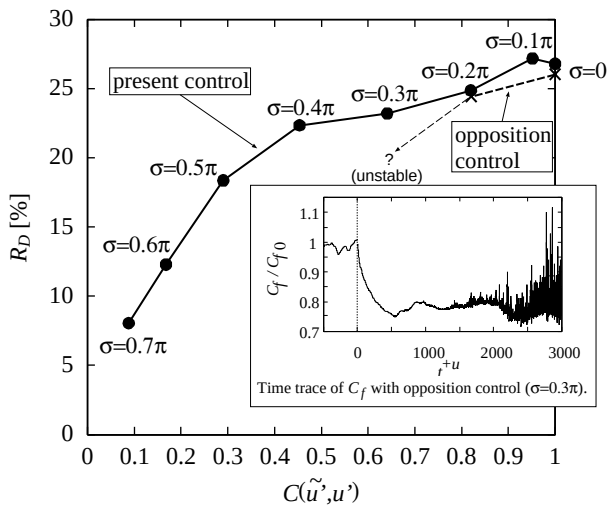

Fig. 7 Effect of de-correlation on drag reduction rate ($y_d^{+u} \simeq 15$, $\alpha = 0.15$).

the streamwise velocity fluctuations in the detection plane (i.e., above the wall) is perfectly known. In the followings, investigation is made for the cases where the sensor signal is artificially deteriorated by the random phase shift, i.e., Eq. (5), and discussion is made toward the implementation of present control scheme in the practical situations where information is available only on the walls.

Figure 7 shows the relation between the amount of random phase shift to the drag reduction rate. The simulation is repeated with different standard deviations of phase shift, σ. In the figure, R_D is drawn as a function of resultant correlation coefficient, $C(\tilde{u}',u')$, of the true and deteriorated (i.e., random phase-shifted) streamwise velocity fluctuations at $y^{+u} \simeq 15$. The drag reduction rate is kept at the same level (i.e., around 25 %) when $C(\tilde{u}',u')$ is larger than 0.45, while it rapidly decreases for $C(\tilde{u}',u') < 0.45$. This result suggests that around 25 % drag reduction is attainable by using the wall information only, if the streamwise velocity fluctuation can be estimated with a correlation coefficient, C, larger than 0.5, by using an advanced state estimation technique.

For comparison, *v*-control with the random phase shift was also examined. If the drag reduction rate is kept at the same level, similarly to the present control, *v*-control can also become a good candidate to be used with the state estimation technique. For $\sigma = 0.2\pi$ ($C \simeq 0.8$), the drag reduction rate is at the same level as the case with $C = 1$. For $\sigma > 0.2\pi$ ($C < 0.8$), however, the computation became unstable after reaching the quasi-steady state, as exemplified by the time trace of C_f in the small figure embedded in Fig. 7. Whether the cause for this instability is physical or numerical (or coupled) is not yet known. In the case of present control, such an instability did not

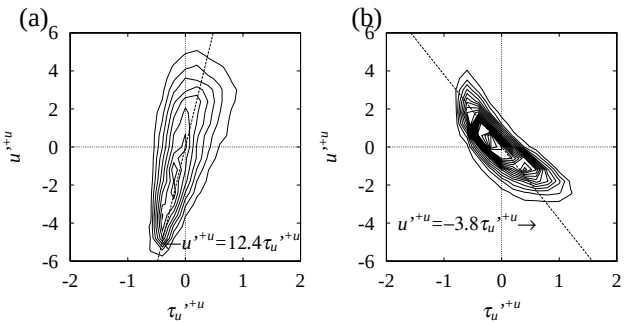

Fig. 8 Joint PDF of streamwise wall shear fluctuation ($\tau_u'^{+u}$) and streamwise velocity fluctuation at $y^{+u} \simeq 15$ (u'^{+u}): (a) without control; (b) with present control ($y_d^{+u} \simeq 15$, $\alpha = 0.15$, $\sigma = 0$).

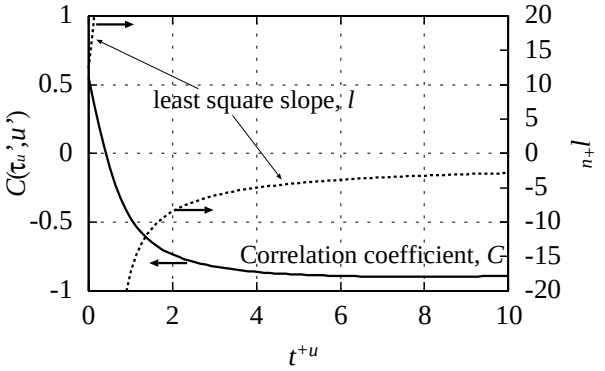

Fig. 9 Time trace of the correlation coefficient, $C(\tau_u',u')$, and the least square slope, l, at the initial stage of present control ($y_d^{+u} \simeq 15$, $\alpha = 0.15$, $\sigma = 0$).

appear for any values of σ.

It can be easily imagined that the streamwise velocity fluctuations around $y^+ \simeq 15$ is correlated fairly well with the streamwise wall shear fluctuation (τ_u'). Therefore, the most straightforward way to estimate u' may be to assume a linear relation, i.e.,

$$u' = l\,\tau_u' \,, \tag{7}$$

where l is a coefficient.

Figure 8 shows the joint probability density function (jPDF) of τ_u' and u'. Before the control is applied, τ_u' and u' have a strong positive correlation. The correlation coefficient, $C(\tau_u',u')$, is about 0.5. The line shown in the figure is the line of Eq. (7), in which the coefficient, l, is determined by the least square method. In the quasi-steady state with the present control ($y_d^{+u} \simeq 15$, $\alpha = 0.15$), the correlation is also strong, but it changes to a negative correlation ($C(\tau_u',u') \simeq -0.8$).

The change of sign in $C(\tau_u',u')$ implies that there is a time-period where the correlation between τ_u' and u' is around zero. As shown in Fig. 9, such a time-period

appears immediately after the onset of control (within one wall unit time), The time trace of the least square slope, l^{+u}, also shown in the figure, indicates that the distribution of the jPDF turns anticlockwise from Fig. 8(a) to Fig. 8(b). Due to this uncorrelated time-period, it would difficult be to attain drag reduction by using the simple linear estimation from the streamwise wall shear stress, i.e., Eq. (7), and therefore a more advanced estimation technique is required.

5. Conclusions

We proposed a new idealized feedback control scheme for skin friction drag reduction in wall-bounded turbulent flows. The control scheme uses streamwise velocity information above the wall, and the control input (i.e., blowing/suction from the wall) is applied so as to suppress the Reynolds shear stress.

The DNS of turbulent pipe flows at $Re_b = 5300$ with the present control showed over 25 % drag reduction. The dependency of the drag reduction rate on the detection plane height is similar to that of the opposition control proposed by Choi et al. [(4)].

The numerical tests with the deteriorated sensor signal showed that over 20 % drag reduction can be attained when the information used for control is fairly well correlated with the desired information (i.e., correlation coefficient larger than 0.5). This result suggests high possibility for the present control scheme to be implemented in practical applications with an advanced state estimation technique.

It was also found that that the streamwise velocity fluctuation above the wall is negatively correlated with the streamwise wall shear fluctuation, which indicates a difficulty of the use of simple linear estimation during the initial stage of control.

Acknowledgments

This work was supported through the Project for Organized Research Combination System by the Ministry of Education, Culture, Sports and Technology of Japan (MEXT). The first author (KF) was also partly supported through the Grant-in-Aid for Young Scientists (B) by MEXT.

References

(1) Kasagi, N., Progress in Direct Numerical Simulation of Turbulent Transport and Its Control, Int. J. Heat Fluid Flow, Vol. 19, No. 2 (1998), p. 125-134.

(2) Kim, J., Control of Turbulent Boundary Layers, Phys. Fluids, Vol. 15, No. 5 (2003), p. 1093-1105.

(3) Bewley, T. R., Moin, P. and Temam, R., DNS-Based Predictive Control of Turbulence: An Optimal Benchmark For Feedback Algorithms, J. Fluid Mech., Vol. 447 (2001), p. 179-225.

(4) Choi, H., Moin, P. and Kim, J., Active Turbulence Control for Drag Reduction in Wall-Bounded Flows J. Fluid Mech., Vol. 262 (1994), p. 75-110.

(5) Hammond, E. P., Bewley, T. R. and Moin, P., Observed Mechanisms for Turbulence Attenuation and Enhancement in Opposition-Controlled Wall-Bounded Flows, Phys. Fluids, Vol. 10, No. 9 (1998), p. 2421-2423.

(6) Iwamoto, K., Suzuki, Y. and Kasagi, N., Reynolds Number Effect on Wall Turbulence: Toward Effective Feedback Control, Int. J. Heat Fluid Flow, Vol. 23, No. 5 (2002), p. 678-689.

(7) Fukagata, K. and Kasagi, N., Drag Reduction in Turbulent Pipe Flow with Feedback Control Applied Partially to Wall, Int. J. Heat Fluid Flow, Vol. 24, No. 4 (2003), p. 480-490.

(8) Lee, C., Kim, J., Babcock, D. and Goodman, R., Application of Neural Networks to Turbulence Control for Drag Reduction Phys. Fluids, Vol. 9, No. 6 (1997), p. 1740-1747.

(9) Lee, C., Kim, J. and Choi, H., Suboptimal Control of Turbulent Channel Flow for Drag Reduction J. Fluid Mech., Vol. 358 (1998), p. 245-258.

(10) Fukagata, K., Iwamoto and K., Kasagi, N., Contribution of Reynolds Stress Distribution to the Skin Friction in Wall-Bounded Flows, Phys. Fluids, Vol. 14, No. 11 (2002), p. L73-L76.

(11) Fukagata, K. and Kasagi, N., Suboptimal Control for Drag Reduction via Suppression of Near-Wall Reynolds Shear Stress, Int. J. Heat Fluid Flow, Vol. 25, No. 3 (2004), p. 341-350.

(12) Yoshino, T., Suzuki, Y., Kasagi, N. and Kamiunten, S., Optimal Thermal Design of Micro Hot-film Wall Shear Stress Sensor, Trans. Jpn. Soc. Mech. Eng., (in Japanese), Vol. 70, No. 689 (2004), p. 38-45.

(13) Milano, M. and Koumoutsakos, P., Neural Network Modeling for Near Wall Turbulent Flow, J. Comput. Phys., Vol. 182, No. 1 (2002), p. 1-26.

(14) Bewley, T. R. and Protas, B, Skin Friction and Pressure: The "Footprints" of Turbulence, Physica D, Vol. 196 (2004), p. 28-44.

(15) Hœpffner, J., Control and Estimation of Wall Bounded Flow Systems, TRITA-MEK Technical Report, 2004:10 (Licentiate Thesis), Kungl. Tekniska Högskolan, Stockholm (2004).

(16) Fukagata, K. and Kasagi, N. Highly Energy-Conservative Finite Difference Method for the Cylindrical Coordinate System, J. Comput. Phys., Vol. 181, No. 2 (2002), p, 478-498.

(17) Spalart, P. R., Moser, R. D. and Rogers, M. M., Spectral Methods for the Navier-Stokes Equations with One Infinite and Two Periodic Directions, J. Comput. Phys., Vol. 96, No. 2 (1991), p. 297-324.

(18) Dukowicz, J. K. and Dvinsky, A. S, Approximate Factorization as a Higher-Order Splitting for the Implicit Incompressible Flow Equations, J. Comput. Phys., Vol. 102, No. 2 (1992), p. 336-347.